THE JOURNAL OF PHYSICAL CHEMISTRY C

pubs.acs.org/JPCC Article

Spin Dynamics in Mn:ZnSe Quantum Dots: A Pulsed High-Frequency EPR Study

Jasleen K. Bindra, Kedar Singh, Johan van Tol, Naresh S. Dalal, and Geoffrey F. Strouse*

Cite This: J. Phys. Chem. C 2020, 124, 19348−19354 Read Online

ACCESS | Metrics & More | Article Recommendations | Supporting Information

ABSTRACT: Dilute magnetic semiconductor quantum dots (DMSQDs) have emerged as potential materials for future spin-based technologies. A critical parameter for the development of this technology is a relatively long electron spin phase memory time, T_2, which could be gleaned from relaxation measurements via pulsed EPR (pEPR). T_2 must be long enough for the data storage and manipulation processes. Thus, pEPR studies of lightly doped quantum dots (QDs) have recently yielded important spin dynamical data on DMSQDs. The earlier studies have, however, been carried out mostly at 3.5 T and 9.5 GHz. Since relaxation dynamics depend sensitively on the Zeeman field and temperature, this work reports the use of higher microwave frequencies up to 240 GHz, in continuous wave (CW) and pEPR modes. The samples studied are ∼2 nm 0.8, 1.6, 3.2% Mn-doped ZnSe QDs. Unlike at 9.5 GHz, the use of higher frequencies enables us to resolve EPR peaks from surface and core sites. A detailed examination of the temperature and frequency dependence of the spin−lattice relaxation time T_1 across a wide range of temperatures (1.8−20 K) and frequencies (9.7−240 GHz) revealed that the relaxation mechanism involves the direct processes. The T_1 decay is found to be bimodal, in contrast to the earlier low-frequency data. Additionally, the observation of large T_2 times and Rabi oscillations indicates that Mn spins in the doped ZnSe QDs can be successfully manipulated and thus be promising components in quantum computation devices.

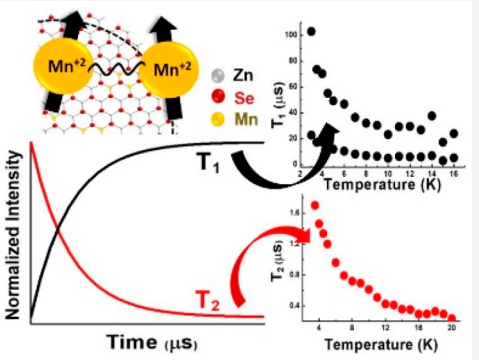

INTRODUCTION

There is significant interest in designing materials that exhibit long-range spin coupling with long coherence times for applications in quantum computing. Such materials include large-spin magnetic molecules, nitrogen-vacancy centers in diamond, and dilute magnetic semiconducting quantum dots (DMSQDs).[1−5] The static spin properties of Mn^{2+} isovalent doped quantum dots have been studied extensively in recent years; however, measurements of the spin dynamics have been studied less extensively.[2−7] The utilization of DMSQDs in spin-based technologies requires a more detailed study of the spin dynamics.

A direct method for investigating spin dynamics of paramagnetic ions is pulsed electron paramagnetic resonance spectroscopy (pEPR). Gamelin and co-workers[2−4] applied low-frequency (X-band, 3.5 T Zeeman field) pEPR to observe the average Rabi oscillations for the statistical distribution of Mn^{2+} sites that arise in Mn-doped ZnO, ZnSe, and CdSe DMSQDs.[2−4]

Recent studies using continuous electron paramagnetic resonance spectroscopy (cwEPR) have shown high-frequency EPR allows the unique Mn^{2+} sites to be identified in Mn-doped II−VI QDs.[6,7] The use of multifrequency EPR spectroscopy allows for a more in-depth study of the spin dynamics in Mn-doped ZnSe QDs. The low-frequency studies demonstrate that the spin dynamics are governed by spin−lattice interactions impacted by surface nuclei,[3] addition of conduction band electrons,[4] and surface passivation.[3] The observed Rabi oscillations and their analysis in terms of Rabi frequency provided support of the potential of DMSQDs in terms of spin−orbit operation time and the coherence time, which sets the error correction window.[2] Since spin−lattice relaxation is strongly dependent on the Zeeman field and sample temperature, studies at much higher frequencies (hence magnetic fields) and variable temperature are needed to assess the spin dynamics in these DMSQDs and their potential applications to spin-based technologies.

In this article, frequency-dependent continuous and pulsed EPR (cwEPR and pEPR) measurements were carried out to elucidate the spin−lattice and spin−spin relaxation times (T_1 and T_2) for a series of hexadecylamine passivated 2 nm $Mn_xZn_{1-x}Se$ DMSQDs (x = 0.008, 0.016, and 0.032). The observed T_1 and T_2 relaxation behavior provides evidence of the T_1 relaxation being dominated by Mn^{2+} donor levels in the

Received: June 3, 2020
Revised: July 24, 2020
Published: July 27, 2020

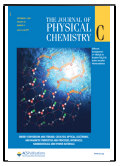

Downloaded via FLORIDA STATE UNIV on March 2, 2026 at 19:18:29 (UTC).
See https://pubs.acs.org/sharingguidelines for options on how to legitimately share published articles.

ACS Publications © 2020 American Chemical Society

https://dx.doi.org/10.1021/acs.jpcc.0c05011
J. Phys. Chem. C 2020, 124, 19348−19354

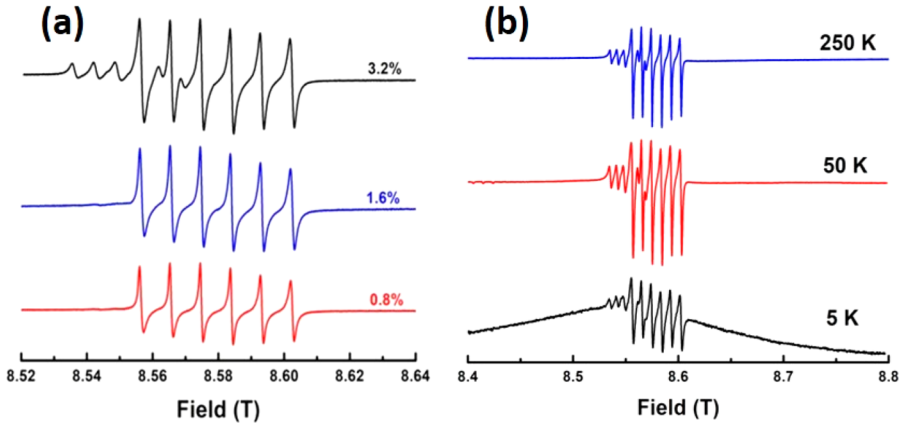

Figure 1. EPR spectra of 2 nm Mn:ZnSe QDs showing (a) concentration dependence at 240 GHz and (b) temperature dependence of 3.2% Mn doped at 240 GHz.

bandgap, as evidenced by a T_1 relaxation mechanism. Unique relaxation rates and oscillations (11 and 15 MHz) are observed in the Mn:ZnSe QDs. The 11 MHz is a Rabi oscillation, while the 15 MHz is assigned as an ESSEM effect arising from Mn—surface ligand interactions. The two decay profiles are assigned to Mn center associated surface and core sites based on the cw and pulsed experiments, as well as comparison to prior results in related II–VI QD systems.[6,7] The cw HFEPR experiments reveal unique g and A values. The population ratio of the surface and core Mn^{2+} sites scales with the dopant concentration; however, the concentration-dependent EPR measurements suggest that the Mn^{2+} guest ions primarily occupy the surface sites at low concentrations and exhibit increased core population with increasing concentration.

RESULTS AND DISCUSSION

A series of spherical, 2 nm hexadecylamine passivated $Mn_xZn_{1-x}Se$ DMSQDs were prepared with manganese concentrations of 0.8, 1.6, and 3.2% through the reaction of $Li_4[Zn_{10}Se_4(SC_6H_5)_{16}]$ (Zn_{10}) and $MnCl_2$ in hexadecylamine (HDA), as reported previously.[9] The QD samples were characterized by standard techniques (Supporting Information Figure S1). The Mn^{2+} incorporation onto Zn^{2+} sites will be an average of 1 for 0.8%, 2 for 1.6%, and 4 for 3.2% Mn^{2+}.[6,7] Based on previous studies, it is anticipated that the Mn^{2+} distribution will reflect a Poisson distribution between the QD core and surface[10] and can be evaluated using continuous wave high-frequency EPR (HFEPR).

In Figure 1a, the concentration-dependent EPR are shown at 240 GHz and 250 K for the $Mn_xZn_{1-x}Se$ samples. The frequency-dependent spectra at 9.8, 120, and 240 GHz are available in the Supporting Information Figures S2A and B. The EPR pattern of the 3.2% sample can be simulated as two independent overlapping sextet patterns that are frequency resolvable. In analogy to earlier work on Mn:CdSe QDs,[5,6] the two patterns can be assigned to a distorted surface site (site 2) and a cubic core site (site 1). Site 1 is represented as a Mn^{2+} center surrounded by four Se atoms in the wurtzite crystal. Site 2 is a distorted site assigned to a surface site.

Parameterization of the EPR spectra is possible since as an isoelectronic cation dopant at the tetrahedral Zn^{2+} site in wurtzite ZnSe QDs, the half-filled d^5 Mn^{2+} ion will exhibit a sextet hyperfine splitting pattern in the HFEPR spectrum, reflecting the $S = 5/2$, $I = 5/2$, $L = 0$ ground state ($^6A_1$).[11] The six electronic spin levels lead to five electronic transitions, of which only the $m_s = -1/2$ to $m_s = +1/2$ shows the resolved ^{55}Mn hyperfine splitting. The other four transitions are broadened by zero-field splitting according to

$$\vec{H} = \sum \left[g\beta\vec{B}\vec{S} + A\vec{I}\vec{S} + D\left(S_z^2 - \frac{\vec{S}^2}{3}\right) + E(S_x^2 - S_y^2) \right] \quad (1)$$

The hyperfine term $A \approx (\chi_0)\alpha^2$ is the isotropic contact term where $\chi_0 = g_e^{-1}g_n^{-1}\langle r^3\rangle$, g_e and g_n are the electron and nuclear g values, r is the radial extension of the sp–d hybrid orbital, and α is a first-order perturbation term related to sp–d orbital admixture.[7,8,12] The zero-field splitting (ZFS) parameters D and E are zero in a tetrahedral (cubic) environment but will be nonzero in a distorted environment. The D parameter is treated as a distribution of dipole–dipole interactions reflecting the statistical incorporation of Mn^{2+} centers, as reported by a D-strain parametrization. We have neglected fourth and higher order crystal field terms, as they are much smaller than the observed strains in D and E, and the rest of the symbols have their standard meaning.

From Figure 1, the extracted EPR parameters for site 1 and site 2 are $g_1 = 2.0072$ and $g_2 = 2.001$, hyperfine constants $A_1 = 197$ MHz and $A_2 = 257$ MHz, and zero-field splitting parameters $D_1 = 0.1$ GHz (± 0.02) GHz, $D_2 = 0.06 \pm 0.04$ GHz, and $\Delta D_2 = 0.065$ GHz. The larger error in the latter value is consistent with a higher structural disorder.[6,7] An observed increase in the g value relative to the free-electron value is evidence of increased host lattice covalency. Distortion in site 2 is confirmed by inspection of the larger hyperfine term (A_2) and the broadened line shape. Enhanced hyperfine splitting is a signature Mn^{2+} located at or near the QD surface.[12] The larger A term for site 2 can be interpreted in terms of a reduced covalence and hence larger spin density on the Mn^{2+}.

The difference in line shape for the two sites in the EPR pattern reflects the distribution of Mn^{2+} local sites within the ZnSe QD as evidenced by the magnitude of the D strain. Since the energy due to the D term is proportional to m_s^2, the outermost peaks will broaden much more than the central peak, which involves the $m_s = -1/2$ to $m_s = +1/2$ transition for a system experiencing different environments. A single site is observed consistent with site 2 (surface) at 0.8 and 1.6%, as shown in the Supporting Information (Figure S2). The experimental observations imply the Mn^{2+} may prefer passivant

https://dx.doi.org/10.1021/acs.jpcc.0c05011
J. Phys. Chem. C 2020, 124, 19348–19354

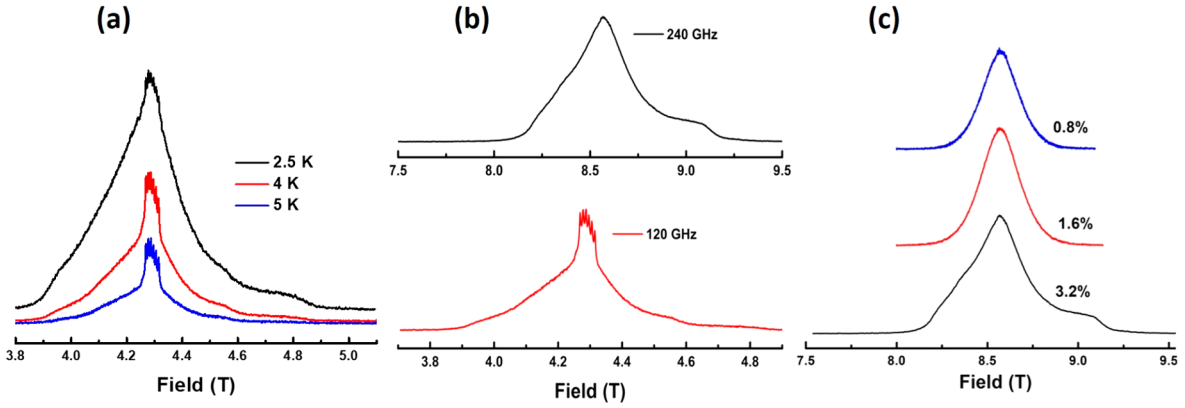

Figure 2. Electron spin echo intensity versus magnetic field measured at time delay $\Delta\tau = 0$ for different (a) temperatures at 120 GHz, (b) frequencies of 3.2% of Mn dopant, and (c) concentrations at 240 GHz in 2 nm Mn:ZnSe QDs at 5 K.

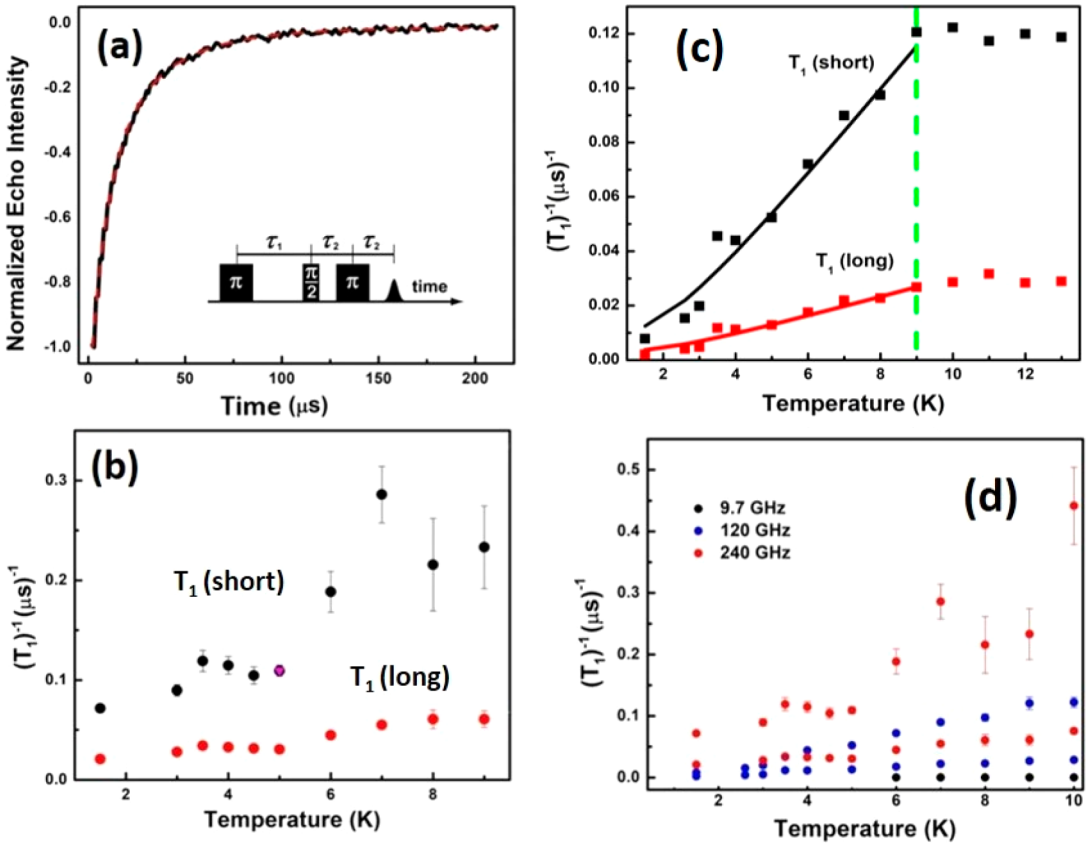

Figure 3. Spin echo decay using an echo-detected inversion recovery sequence (black) and biexponential fit (red) to obtain $(T_1)^{-1}$ (a). Temperature dependence of short (black) and long (red) $(T_1)^{-1}$ (b). 240 GHz for 3.2% Mn:ZnSe QDs. Temperature dependence of short (black) and long (red) $(T_1)^{-1}$ at 120 GHz for 3.2% Mn:ZnSe QDs with their respective fits in solid lines. (c) Temperature dependence of $T_1(d)$ for different frequencies..

coordination at low concentration and potentially reflect the effect of cluster-oriented addition, as suggested by Snee et al.[13]

The temperature-dependent EPR spectrum for the 3.2% sample is shown in Figure 1b. The data for the 0.8 and 1.6% sample are shown in the Supporting Information. The spectra exhibit changes in the spectral shape which can be accounted for by considering the magnitude of kT relative to the value for $g\mu_B B$. In the EPR spectrum at 250 K, when $kT \gg g\mu_B B$, the population differences are about equal for all five m_s transitions resulting in a derivative EPR spectrum dominated by the $m_s = -1/2$ to $m_s = +1/2$ transition. At 5 K, the EPR spectrum is in the limit $kT \ll g\mu_B B$ leading to a population difference between the $m_s = -5/2$ and $m_s = -3/2$ transition being appreciable with distribution of Mn^{2+} sites, as evidenced by the presence of the broad component observed in the low-temperature spectrum.

The presence of multiple sites for Mn^{2+} is observed in the echo-detected (ED) field sweep EPR spectra measured at time delay $\Delta\tau = 0$ for the 3.2% Mn:ZnSe collected at 240 GHz from 7.5 to 9.5 T. It is important to note that in the ED experiments, the field window is significantly larger than the cwEPR, and as the temperature is lowered the hyperfine features decrease in

https://dx.doi.org/10.1021/acs.jpcc.0c05011
J. Phys. Chem. C 2020, 124, 19348−19354

Table 1. Frequency and Concentration Dependence of T_1 and T_2 for 0.8, 1.6, and 3.2% Mn-Doped 2 nm ZnSe QDs at 5 K

	9.7 (GHz)			120 (GHz)			240 (GHz)		
	0.8	1.6	3.2	0.8	1.6	3.2	0.8	1.6	3.2
$T_{1(\text{short})}$ (μs)	26	21	26	11	12	19	9.5	9.1	9.2
$T_{1\ (\text{long})}$ (μs)	184	118	192	55	49	78	41	37	33
T_2 (μs)	0.84	–	–	1.1	1.2	1.6	1.5	1.7	2.0

intensity due to the decrease of population in the $m_s = -1/2$ to $m_s = +1/2$ transition and D strain in the system leading to broadening of the five $\Delta m_s = \pm 1$ EPR transitions.

The temperature- (Figure 2a) and frequency- (Figure 2b) dependent data for the 3.2% sample are presented in Figure 2, while temperature- and frequency-dependent ED-EPR data for 0.8% and 1.6% are available in the Supporting Information (Figure S3). In Figure 2a, multiple Mn^{2+} sites are present in the EPR data with features identifiable at 3.97, 4.28, and 4.75 T. The features are better resolved at low temperature but occur at the same position, as expected for D-strain contributions. The presence of multiple sites is further shown in the frequency-dependent data (Figure 2b), where the impact of the higher frequency on resolution allows differentiation of the local Mn^{2+} sites.

In Figure 2c, the concentration-dependent EPR spectra at 5 K (240 GHz) are plotted. The 0.8% Mn^{2+} has a symmetric Gaussian peak shape at 8.25 T, but as illustrated in the data the signal becomes more and more asymmetric as the concentration of the dopant ion is increased. The asymmetry is a measure of the increased number of sites present and the increased Mn−Mn dipole−dipole interaction arising at higher Mn^{2+} concentrations, consistent with the expected behavior for a statistical distribution of Mn^{2+} throughout the $Mn_xZn_{1-x}Se$ QD.

The frequency- and temperature-dependent experimental cw and ED data support a model wherein Mn^{2+} occupies local distorted four-coordinate T_d cation sites within the ZnSe QD lattice. Whether the distortions reflect vacancy or layer differences is not distinguishable. The assignment of the sites to a reconstructed surface and a unique core is consistent with earlier reports (NMR in CdSe[14] and EPR in Mn:CdSe),[6,7] where the outer two layers of the QD are observed to relax to lower strain reflecting ligation of dangling sites.

Spin Relaxation. It is reasonable to assume that the T_1 and T_2 relaxation pathways for the Mn^{2+} local sites should be site dependent. To evaluate the individual site behavior for T_1 and T_2, spin relaxation measurements were performed at 8.25, 8.57, and 9.06 T at 240 GHz for the 0.8, 1.6, and 3.2% samples. The normalized echo-detected inversion recovery signal at 8.25 T, 5 K (240 GHz) for 3.2% Mn:ZnSe QDs is shown in Figure 3a. Experimental data for the 0.8 and 1.6% samples are available in the Supporting Information (Figure S4).

Temperature dependence of the T_1 relaxations is shown in Figure 3b and tabulated in Table 1. The value of T_1 is measured by monitoring the recovery of longitudinal magnetization using an echo-detected inversion recovery sequence ($\pi-\tau_1-\pi/2-\tau_2-\pi-\tau_2-$echo) while τ_1 is varied. The value of T_2 is analyzed using a Hahn echo sequence ($\pi/2-\tau-\pi-\tau-$echo). The widths of the pulses are carefully adjusted between 200 and 400 ns to maximize the echo signals. T_1 values are obtained by fitting the echo decay with a biexponential function ($a_1e^{-\tau/T_1\text{short}} + a_2e^{-\tau/T_1\text{long}}$) in order to account for the presence of two pathways for spin−lattice relaxation.

In Figure 3c, the temperature dependent $(T_1)^{-1}$ is plotted for 3.2% Mn:ZnSe measured at 120 GHz. The long (black) and short (red) T_1 for the 3.2% sample is fit for temperatures below 9 K using a model that incorporates contributions from a direct phonon relaxation process, where[11] $(T_1)^{-1} \propto \coth(h\nu/2kT)$.

$$T_1^{-1} = C_1\coth(h\nu/2kT) + C_2 \quad (2)$$

In eq 2, $h\nu$ is the energy of a photon absorbed or a photon emitted in a resonance transition. Figure 3d shows the temperature dependence of $(T_1)^{-1}$ at different frequencies for 3.2% Mn:ZnSe. The values of frequency and concentration dependence of T_1 and T_2 for 0.8, 1.6, and 3.2% Mn-doped 2 nm ZnSe QDs at 5 K, 9.7, 120, and 240 GHz are listed in Table 1. Table 2 shows extracted values of prefactor C_1 which

Table 2. Parameters Obtained by Fitting Spin−Lattice Relaxation Rates vs Temperature by Using Eq 2 for 0.8, 1.6, and 3.2% Mn-Doped ZnSe QDs

	120 (GHz)			240 (GHz)		
	0.8	1.6	3.2	0.8	1.6	3.2
C_1 (short) (μs^{-1})	0.04	0.06	0.05	0.13	0.14	0.15
C_1 (long) (μs^{-1})	0.008	0.014	0.010	0.026	0.033	0.039

were obtained by fitting temperature dependence of spin−lattice relaxation rates using eq 2to be frequency dependent. The C_2 parameter for respective concentrations was fixed to the corresponding relaxation rates obtained at the X-band, where the direct process plays less of a role.

The frequency dependence of C_1 may reflect contributions associated with phonon population, population of electronic defect levels lying near the VB or CB edge, or a combination as the population of defect levels is moderated by the presence of lattice phonons, as reported in similar systems.[15,16] Previous studies in nitrogen-doped diamond have reported the participation of lattice phonon contributions to spin relaxation.[17] For a phonon-dominated process, the direct relaxation rate will exhibit a frequency square dependence, reflecting the approximation of an energy square dependence of the phonon density of states. For an electronic defect the dependence will be related to doping level and phonon density. Assuming the electronic defect levels introduced by Mn^{2+} incorporation dominate the defect-scattering center, the observed frequency dependence can also be attributed to an intraband relaxation process,[18] as shown in Figure 4. In Mn-doped ZnSe QDs we believe this is the most likely mechanism, consistent with the observation of a concentration-dependent response, T_1 longitudinal relaxation behavior. Furthermore, the existence of Mn^{2+} energy levels lying between the VB−CB levels has been reported. The coparticipation of phonons is likely, as the bath of vibrational states in the QD and at the surface will allow efficient relaxation pathways. A definitive mechanism cannot be assigned due to the limited frequency range studies in this article.

https://dx.doi.org/10.1021/acs.jpcc.0c05011
J. Phys. Chem. C 2020, 124, 19348−19354

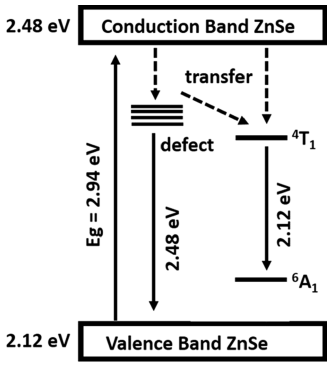

Figure 4. Energy level diagram for Mn-doped ZnSe QDs.

The field-dependent spin−spin relaxation or transverse relaxation is plotted in Figure 5a at 5 K (240 GHz). The temperature dependence for this spin−spin relaxation rate $(T_2)^{-1}$ is plotted in Figure 5b and as a function of frequency in 120 and 240 GHz is plotted in Figure 5c. T_2 is obtained using a single-exponential function $(ae^{-2\tau/T_2})$. The data for T_2 are summarized in Table 1. The behavior of T_2 can be accounted for by the enhanced Mn−Mn dipole−dipole interactions as the probability of nearest-neighbor pairs increase in the lattice, coupled to the predominant coupling between Mn^{2+} centers being governed by a RKKY carrier-mediated coupling process, as reported in Mn:CdSe QDs.[19]

Rabi Oscillations. The relaxation behavior is important to the potential application in Q-bits and is evaluated by measuring its Rabi frequency, which determines the operation time and its coherence time, setting the error correction window.[2] For EPR transitions, the Rabi frequency is proportional to the magnetic dipole transition matrix element $(\Omega_R \propto \langle i|\hat{S}_+|f\rangle)$.[2]

In Figure 6, nutation experiments for 0.8 and 1.6% $Mn_xZn_{1-x}Se$ QDs are shown along with their respective Fourier transforms. The spectra are recorded at 5 K, 9.7 GHz. Rabi oscillations were observed with more than one oscillation frequency at higher concentration. Consistent with the T_1 and cw EPR experiments, the Rabi oscillation consists of two main frequencies (at ∼11 and 15 MHz). The peak at 15 MHz is assigned to an electron spin echo envelope modulation (ESEEM) and is not assigned as an independent Rabi oscillation.[2]

The ESSEM contributions are believed to arise from nuceli−nuiclei interactions reflecting surface ligand contributions. The interactions are apparent from the periodic oscillations of the echo intensities in Figure 6b (inset) and become much clearer after subtracting the fit as observed in Figure 6b (inset) at higher dopant concentrations. The dominant oscillation frequency at this field is 14.68 MHz, close to the ^1H Larmor frequency at this field (14.8 MHz). Further studies are underway to evaluate the relaxation times. The observed relaxation times are of same order of magnitude as materials with applications in quantum computing.[2−5,15]

CONCLUSIONS

Multifrequency EPR was used as a tool to investigate spin dynamics in ∼2 nm Mn-doped ZnSe QDs. Temperature and frequency dependence of T_1 and T_2 was measured. Both relaxation times show a strong temperature and magnetic field dependence, indicating these thermodynamic parameters can provide a sensitive handle on the spin dynamics and thus the

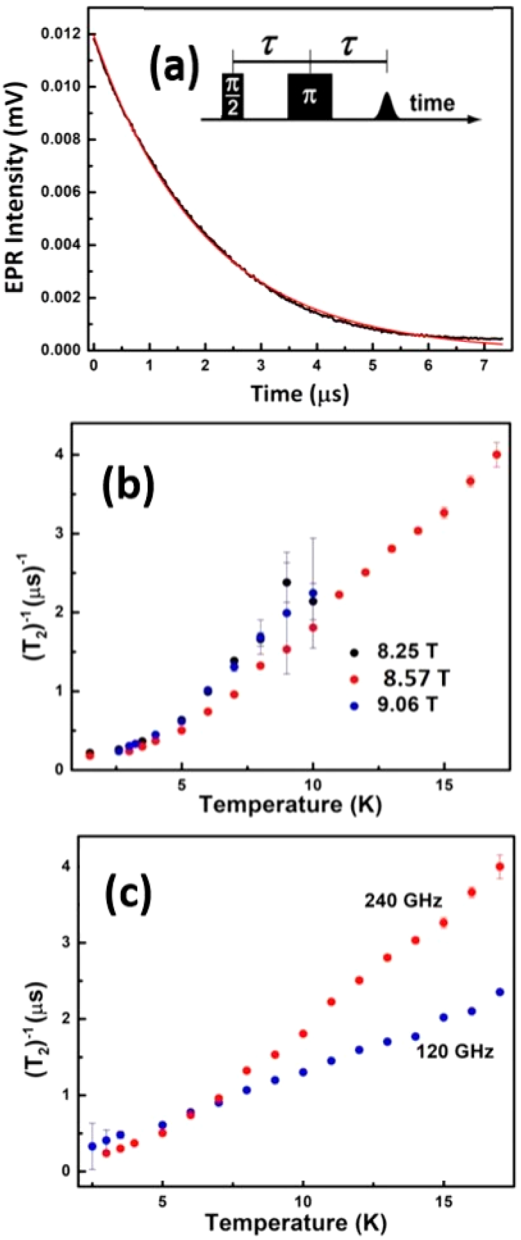

Figure 5. Spin−spin relaxation (T_2) experimental (black) and fit (red) with pulsed sequence used (inset) at 5 K, 240 GHz (a) and temperature dependence of $(T_2)^{-1}$ (b) at 240 GHz for 3.2% Mn:ZnSe QDs. Temperature dependence of $(T_2)^{-1}$ (c) for different frequencies.

decoherence times of the family of the ZnSe:Mn DMSQDs. T_1 shows a biexponential behavior for all frequencies, and T_2 exhibits monoexponential decay. While the T_1 shortens with increasing frequency due to the contribution of the single phonon direct process, the T_2 at low temperature is longer at higher frequencies with the decrease of spin flip-flop events at higher spin polarization.[20]

The observed relaxation behavior in Mn-doped ZnSe QDs suggests that dopant engineering in DMSQDs and a judicious choice of magnetic fields and frequencies can lead to potential applications in quantum computation.

https://dx.doi.org/10.1021/acs.jpcc.0c05011
J. Phys. Chem. C 2020, 124, 19348−19354

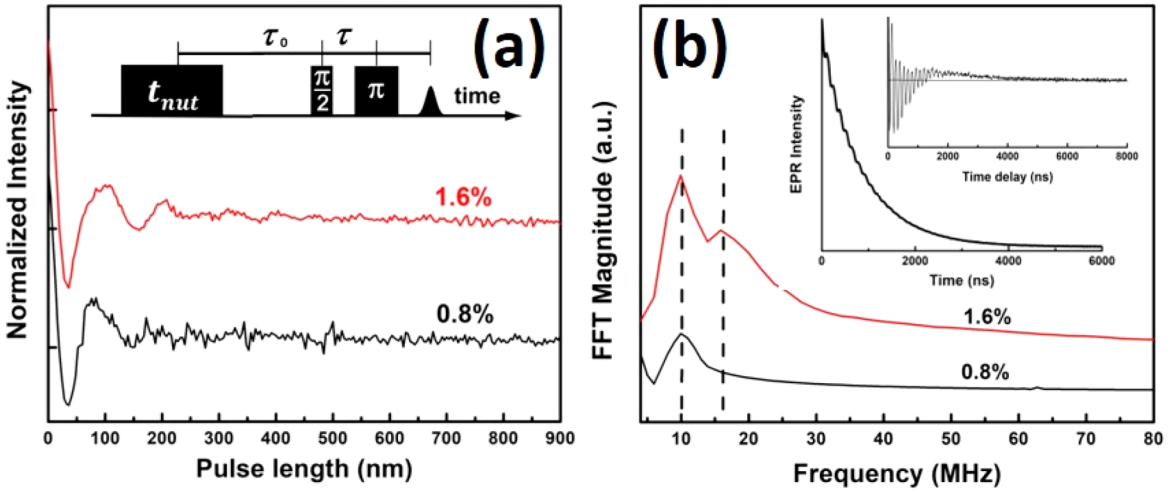

Figure 6. Rabi oscillations (a) and FFT (b) of 2 nm 0.8 and 1.6% doped Mn:ZnSe QDs at 0.3465 T, 9.7 GHz, 5 K with inset showing oscillation in echo intensities and the difference between experimental and fit in the subinset.

EXPERIMENTAL SECTION

Chemicals. Hexadecylamine (HDA) (90%, Acros Organics), $MnCl_2$ (99.9% Acros Organics), toluene (99.9%, EMD Chemicals), and methanol (99.8%, VWR) were used as supplied. $Li_4[Se_4Zn_{10}(SC_6H_5)_{16}]$ (Zn_{10} cluster) was prepared as previously described[9] of the transition metal salt ($MnCl_2$).

Synthesis. Hexadecylamine (HDA) passivated $Mn_xZn_{1-x}Se$ QDs (x = 0.008, 0.016, and 0.032) were prepared by the dissolution $Li_4[Se_4Zn_{10}(SC_6H_5)_{16}]$ in ∼20 mL of HDA at 110°C under N_2 using a Schlenk line. To the solution 0.8, 1.6 and 3.2 mole % of $MnCl_2$ was added, and the reaction was allowed to stir vigorously for 1 hour to induce cation exchange between the Zn^{2+} of the cluster and the Mn^{2+} from the metal salt. The reaction was then heated to 210°C (50°C/min) to induce QD growth. The temperature was kept below 220°C to avoid Sulphur incorporation. The size of the QDs was monitored using UV-vis spectroscopy. Once the desired size was achieved the solution was cooled to room temperature to halt further growth. The cooled solid samples were then isolated by dissolving in ∼10 mL of toluene, followed by precipitation with ∼15 mL of MeOH, and centrifugation. This process was repeated three times to ensure reagent free particles, and the precipitate was dried under a vacuum at room temperature. Sequential dissolution/precipitation steps have been shown to effectively remove unreacted Mn impurities.

Characterization. The QD size was analyzed by using transmission electron microscopy (TEM) for QDs dispersed on holey carbon (400 mesh) from a toluene solution using a JEOL-2010 microscope operated at 200 kV as shown in Figure S1. The TEM measurements confirm the preliminary size obtained using absorption spectroscopy. Structural analysis and QD size were obtained using pXRD of 10 mg samples on a Rigaku DMAX 300 Ultima 3 Powder X-ray diffractometer (using Cu−Kα λ = 1.5418 Å radiation) as shown in Figure S1.

Electron Paramagnetic Resonance. EPR measurements at X-band ∼9.7 GHz were performed on a Bruker E650 spectrometer which is capable of doing both cw and pEPR measurements. HFEPR spectra were recorded on a superheterodyne quasioptical cw/pEPR spectrometer which is located at the National High Magnetic Field Laboratory in Tallahassee, FL. The system consists of a 12.5 T superconducting magnet, a 120/40 mW 120/240 GHz source, quasioptics, a superheterodyne detection system, and a He flow cryostat.[21,22]

Spectral simulations were performed using the computer program EPRCALC.[23]

ASSOCIATED CONTENT

Supporting Information

The Supporting Information is available free of charge at https://pubs.acs.org/doi/10.1021/acs.jpcc.0c05011.

TEM, XRD, and EPR spectra; temperature dependence of T_1 and T_2 relaxation times (Figures S1−S5) (PDF)

AUTHOR INFORMATION

Corresponding Author

Geoffrey F. Strouse − *Department of Chemistry and Biochemistry, Florida State University, Tallahassee, Florida 32306, United States;* orcid.org/0000-0003-0841-282X; Email: strouse@chem.fsu.edu

Authors

Jasleen K. Bindra − *Department of Chemistry and Biochemistry and National High Magnetic Field Laboratory, Florida State University, Tallahassee, Florida 32306, United States*

Kedar Singh − *School of Physical Sciences, Jawaharlal Nehru University, New Delhi 110067, India;* orcid.org/0000-0002-3425-1970

Johan van Tol − *National High Magnetic Field Laboratory, Florida State University, Tallahassee, Florida 32310, United States*

Naresh S. Dalal − *Department of Chemistry and Biochemistry and National High Magnetic Field Laboratory, Florida State University, Tallahassee, Florida 32306, United States;* orcid.org/0000-0002-9996-6918

Complete contact information is available at: https://pubs.acs.org/10.1021/acs.jpcc.0c05011

Author Contributions

The manuscript was written through contributions of all authors.

Notes

The authors declare no competing financial interest.

https://dx.doi.org/10.1021/acs.jpcc.0c05011
J. Phys. Chem. C 2020, 124, 19348−19354

■ ACKNOWLEDGMENTS

We (G.F.S) thank the National Science Foundation CHE-1608364: SusChEM: Understanding Microwave Interactions to Control Magnetic Nanocrystal Growth from a Single Source Precursor and DMR-1905757: Tuning Plasmonic and Magneto-Plasmonic Behavior in 4-d Transition Metal Doped Indium Oxide, the National High Magnetic Field Laboratory, which is supported by the National Science Foundation via Cooperative Agreements No. DMR-1157490 and DMR-1644779 and the State of Florida.

■ REFERENCES

(1) Cerletti, V.; Coish, W. A.; Gywat, O.; Loss, D. Recipes for spin-based quantum computing. *Nanotechnology* **2005**, *16*, R27−R49.
(2) Ochsenbein, S. T.; Gamelin, D. R. Quantum oscillations in magnetically doped colloidal nanocrystals. *Nat. Nanotechnol.* **2011**, *6*, 112−115.
(3) Schimpf, A. M.; Ochsenbein, S. T.; Gamelin, D. R. Surface contributions to Mn^{2+} spin dynamics in colloidal doped quantum dots. *J. Phys. Chem. Lett.* **2015**, *6*, 457−463.
(4) Schimpf, A. M.; Rinehart, J. D.; Ochsenbein, S. T.; Gamelin, D. R. Charge-State Control of Mn^{2+} Spin Relaxation Dynamics in Colloidal n-Type $Zn_{1-x}Mn_xO$ Nanocrystals. *J. Phys. Chem. Lett.* **2015**, *6*, 1748−1753.
(5) Moro, F.; Turyanska, L.; Wilman, J.; Fielding, A. J.; Fay, M. W.; Granwehr, J.; Patanè, A. Electron spin coherence near room temperature in magnetic quantum dots. *Sci. Rep.* **2015**, *5*, 10855.
(6) Zheng, W.; Wang, Z.; Wright, J.; Goundie, B.; Dalal, N. S.; Meulenberg, R. W.; Strouse, G. F. Probing the local site environments in Mn: CdSe quantum dots. *J. Phys. Chem. C* **2011**, *115*, 23305−23314.
(7) Wang, Z.; Zheng, W.; van Tol, J.; Dalal, N. S.; Strouse, G. F. High-field electron paramagnetic resonance as a microscopic probe of anisotropic strain at Mn^{2+} sites in CdSe: Mn^{2+} quantum dots. *Chem. Phys. Lett.* **2012**, *524*, 73−77.
(8) Furdyna, J. K. J. Diluted magnetic semiconductors. *J. Appl. Phys.* **1988**, *64*, R29−R64.
(9) Lovingood, D. D.; Oyler, R. E.; Strouse, G. F. Composition Control and Localization of S^{2-} in CdSSe Quantum Dots Grown from $Li_4[Cd_{10}Se_4(SPh)_{16}]$. *J. Am. Chem. Soc.* **2008**, *130*, 17004−170011.
(10) Zheng, W.; Strouse, G. F. Involvement of carriers in the size-dependent magnetic exchange for Mn: CdSe quantum dots. *J. Am. Chem. Soc.* **2011**, *133*, 7482−7489.
(11) Abragam, A.; Bleaney, B. *Electron Paramagnetic Resonance of Transition Ions*; Dover Publications: New York, 1986.
(12) Aven, M., Prener, J. S., Eds. *Physics and Chemistry of II−VI Compounds*; North-Holland: Amsterdam, 1967.
(13) Jawaid, A. M.; Chattopadhyay, S.; Wink, D. J.; Page, L. E.; Snee, P. T. Cluster-seeded synthesis of doped CdSe: Cu_4 quantum dots. *ACS Nano* **2013**, *7* (4), 3190−3197.
(14) Berrettini, M. G.; Braun, G.; Hu, J. G.; Strouse, G. F. NMR Analysis of Surfaces and Interfaces in 2-nm CdSe. *J. Am. Chem. Soc.* **2004**, *126* (22), 7063−7070.
(15) Moro, F.; Turyanska, L.; Granwehr, J.; Patane, A. Spin manipulation and spin-lattice interaction in magnetic colloidal quantum dots. *Phys. Rev. B: Condens. Matter Mater. Phys.* **2014**, *90* (20), 205428−205434.
(16) Turyanska, L.; Hill, R. J. A.; Makarovsky, O.; Moro, F.; Knott, A. N.; Larkin, O. J.; Patane, A.; Meaney, A.; Christianen, P. C. M.; Fay, M. W.; Curry, R. J. Tuneable paramagnetic susceptibility and exciton g-factor in Mn-doped PbS colloidal nanocrystals. *Nanoscale* **2014**, *6*, 8919.
(17) Mehra, A. Energy Levels of Divalent Manganese in ZnS. *J. Electrochem. Soc.* **1971**, *118*, 136−138.
(18) Zheng, W.; Strouse, G. F. Involvement of carriers in the size-dependent magnetic exchange for Mn: CdSe quantum dots. *J. Am. Chem. Soc.* **2011**, *133* (19), 7482−7489.
(19) Schweiger, A.; Jeschke, G. *Principles of Pulse Electron Paramagnetic Resonance*; Oxford University Press: New York, 2001.
(20) Takahashi, S.; Hanson, R.; van Tol, J.; Sherwin, M. S.; Awschalom, D. D. Quenching Spin Decoherence in Diamond through Spin Bath Polarization. *Phys. Rev. Lett.* **2008**, *101*, 047601.
(21) Morley, G. W.; Brunel, L. C.; van Tol, J. A Multifrequency High-Field Pulsed Electron Paramagnetic Resonance/Electron Nuclear Double Resonance Spectrometer. *Rev. Sci. Instrum.* **2008**, *79*, 064703−064705.
(22) van Tol, J.; Brunel, L. C.; Wylde, R. J. A Quasioptical Transient Electron Spin Resonance Spectrometer Operating at 120 and 240 GHz. *Rev. Sci. Instrum.* **2005**, *76*, 074101−0741019.
(23) van Tol, J. *EPR Calc*; National High Magnetic Field Laboratory: Tallahassee, FL.

https://dx.doi.org/10.1021/acs.jpcc.0c05011
J. Phys. Chem. C 2020, 124, 19348−19354